Nonstationary magnetization dynamics driven by spin transfer torque

G. Siracusano,[1] G. Finocchio,[1,*] A. La Corte,[2] G. Consolo,[1] L. Torres,[3] and B. Azzerboni[1]
[1]*Dipartimento di Fisica della Materia e Ingegneria Elettronica, University of Messina, Salita Sperone 31, 98166 Messina, Italy*
[2]*Dipartimento di Ingegneria Informatica e delle Telecomunicazioni, University of Catania, Viale Andrea Doria, 6-95125 Catania, Italy*
[3]*Departamento de Fisica Aplicada, University of Salamanca, Plaza de la Merced s/n, 37008 Salamanca, Spain*
(Received 2 November 2008; published 31 March 2009)

This paper shows that the presence of two dynamical regimes, characterized by different precessional axes, is the origin of the nonmonotonic behavior of the output integrated power for large-amplitude magnetization precession driven by spin-polarized current in nanoscale exchange-biased spin valves. In particular, an abrupt loss in the integrated output power exists at the transition current between those two regimes. After the introduction of a time-frequency analysis of magnetization dynamics based on the wavelet transform, we performed a numerical experiment by means of micromagnetic simulations. Our results predicted that, together with a modulation of the frequency of the main excited mode of the magnetization precession, at high nonlinear dynamical regime the instantaneous output power of the spin-torque oscillator can disappear and then reappear at nanosecond scale.

DOI: 10.1103/PhysRevB.79.104438 PACS number(s): 72.25.Ba, 75.20.−g, 75.75.+a

I. INTRODUCTION

The discovery that a spin-polarized current interacting with a nanomagnet can produce several different types of magnetic dynamics[1,2] opens perspectives in applied physics for spintronic technology.[3–8] These offer the possibility of applications that include at least magnetoresistive random access memories,[4] nano-oscillators,[7,9] and radiofrequency detectors.[10] Frequency[7] and time[8] domain measurements of magnetoresistance signal in the "state of the art" spintronic devices (spin valves,[11] magnetic tunnel junctions,[12] point-contact geometries[13]) show very rich dynamical stability diagrams with switching between static magnetic states and different steady-state precessions characterized by uniform and nonuniform magnetization patterns. In particular, the frequency, the linewidth, and the microwave output power of the precessions show strong dependence on external field and current.[14]

In addition, exchange bias nanoscale spin-valves with a Py-free layer ($Py=Ni_{80}Fe_{20}$) of elliptical cross-sectional area exhibit dynamics with series of jumps in frequency between stationary nonlinear modes characterized by either different spatial distribution[15,16] and different Hausdorff dimension.[17] Those measurements also show, for some values of current and field, a nonstationary magnetization dynamics related to nanosecond switching between a dynamical mode and a static magnetic configuration or between different dynamical modes.[16] In the latter case, this nonstationary regime is characterized by a spectrum with two well-defined peaks in frequency, and it is observed before that large-amplitude magnetic precession is driven or when a device is biased near the boundary between the jumps of two different modes. In the large-amplitude dynamical regime, while the frequency of the main excited mode monotonically decreases as function of the current, the integrated output power shows nonmonotonic behavior with a well-defined minimum at least for the device studied in Ref. 15.

Here, we first performed a numerical experiment based on the solution of the Landau-Lifshitz-Gilbert-Slonczewski[18,19] (LLGS) equation in order to identify the origin of the minimum in the integrated output power. Second, we present a continuous wavelet analysis[20] of nonstationary magnetization dynamics driven by spin-polarized current and reproduce the results of nonstationary regime of experimental direct time-domain electrical measurements in nanoscale exchange biased spin-valves obtained for a four-nanosecond windowed Fourier transform. Finally, we predicted by combining micromagnetic simulations and wavelet analysis that the excited modes of a spin-torque nano-oscillator show together to a frequency modulation[21] a nanosecond intermittent disappearing and reappearing of the instantaneous microwave output power.

II. NUMERICAL DETAILS

We simulate exchange-biased spin valves Py(4 nm)(free layer)/Cu(8 nm)/Py(4 nm)(pinned layer)/$Ir_{20}Mn_{80}$/(8 nm) with elliptical cross sectional area (130×60 nm^2) in the same experimental framework of Ref. 16. We use a saturation magnetization $M_S=650\times 10^3$ A/m, a free-layer damping $\alpha_F=0.025$, a pinned layer damping $\alpha_P=0.2$, and an exchange constant of $A=1.3\times 10^{-11}$ J/m.[22] For the spin-torque efficiency $\varepsilon(\theta)$ and the magnetoresistance $r(\theta)$, we use the formulation developed by Slonczewski[23] for symmetric spin valves

$$\varepsilon(\theta)=0.5P\Lambda^2/[1+\Lambda^2+(1-\Lambda^2)\cos(\theta)]$$

and $r(\theta)=[1-\cos^2(\theta/2)]/[1+\chi\cos^2(\theta/2)]$, where $\Lambda^2=\chi+1$, χ is the giant magnetoresistance asymmetry parameter, P is the current spin-polarization factor, and the parameter values $\chi=1.5$ and $P=0.38$ have been obtained by fitting to the experimentally measured ensemble-average switching time.[19] The pinned layer is exchange biased in the plane of the sample at an angle of 45° with respect to the major axis of the ellipse, with an effective exchange field of 75 mT. We simulate the entire spin valve including the effects of the back action of the torque to the pinned layer and a spin

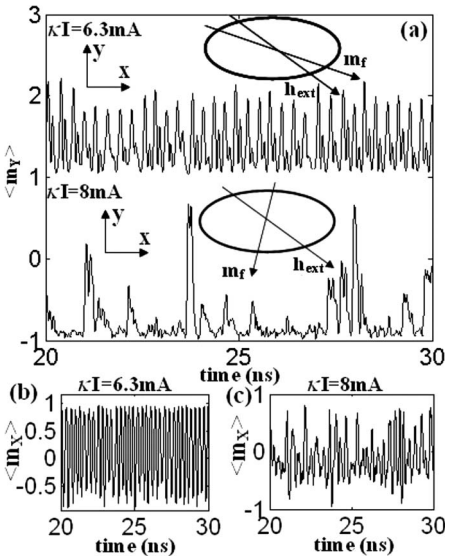

FIG. 1. (a) Temporal evolution of normalized y component of the average magnetization for $\kappa I=6.3$ mA (top, an offset of 2 is applied) and $\kappa I=8$ mA (bottom). The axis of the magnetization oscillation ($\mathbf{m}_f$ in figure) is in the former case between 0° and −45° and in the latter case between −45° and −125°. Temporal evolution of normalized x component of the average magnetization for (a) $\kappa I=6.3$ mA and (b) $\kappa I=8$ mA.

torque with a stochastic component (we include thermal fluctuations also in the pinned layer).[22]

III. RESULTS

In order to qualitatively explain the nonmonotonic behavior of the integrated output power and to compare our numerical results directly to the experimental data (Ref. 15, Fig. 7), we study large-amplitude magnetization dynamics for an external field $\boldsymbol{H}_{\text{ext}}=68$ mT applied along −45° with respect to the easy axis of the ellipse. We identify the proportionality factor (κ) (Ref. 15) between experimental and applied currents (I) by fitting the frequency versus current data; we computed $\kappa=0.34$. The integrated power signal amplitude shows a minimum for a current around 7.5 mA which does not correspond to any nonstationary region or jump between different nonlinear dynamical modes. Near this current value, our results show two different dynamical regimes: those that are characterized by a magnetization oscillation axis [$\mathbf{m}_f$ in Fig. 1(a)] at an angle between 0° and −45° (regime A, lower current) or between −45° and −125° (regime B, larger current). Figure 1 shows the time evolution of the normalized average magnetization [$\langle m_Y\rangle$ (a) and $\langle m_X\rangle$ (b), (c)] for $\kappa I=6.3$ mA in regime A (frequency of the main mode $f=3.3$ GHz) and $\kappa I=8$ mA in regime B ($f=2.8$ GHz). These magnetization time traces are qualitatively similar to the real-time magnetoresistance signal measured via a microwave storage oscilloscope and displayed in Figs. 4(b) and 4(c) of Ref. 16. For large-amplitude magnetization dynamics, first the integrated output power increases as function of current (regime A) then it decreases abruptly (in the transition from regime A to regime B), finally it increases as function of current (regime B). Simulations performed considering the pinned layer fixed did not show these two dynamical regimes; we argue that this is the main point which gives the different results between our micromagnetic simulations and the ones published in Ref. 15.

Concerning the same kind of devices, experimental data published in Ref. 16 show that nonstationary magnetization dynamics is driven before of the large-amplitude magnetization precession. In particular, for $I=4.5$ mA and $\boldsymbol{H}_{\text{ext}}=60$ mT, the power spectrum of the real-time voltage signal [for a signal of 20 ns see Fig. 6(e) in Ref. 16] captured via microwave storage oscilloscope (the voltage is directly proportional to the magnetoresistive signal) shows two excited modes P_1 and P_2 ($f_{P1}=3.9$ GHz and $f_{P2}=4.6$ GHz). By performing the Fourier transform with a window time of 4 ns, either P_1 or P_2 can be observed [see Figs. 6(f) and 6(g) in Ref. 16]. This result shows the nonperiodic origin of this magnetization precession; furthermore the presence of those two modes at second scale also shows their nontransient origin [see Fig. 6(d) in Ref. 16]. From computational point of view, it is important to find out a tool which systematically gives information about the time localization of the excited modes. We use a wavelet-based analysis (the wavelet is the natural generalization of the windowed Fourier transform) and differently by other approaches, we systematically identify the scale set directly from the power spectrum related to $r(t)$ (magnetoresistance time-domain signal). The continuous wavelet transform of a function $r(t)$ (we consider the time dependence of the magnetoresistance signal) is a linear transform $W_r(u,s)$ given by[20]

$$W_r(u,s)=\frac{1}{\sqrt{s}}\int_{-\infty}^{+\infty} r(t)\psi^*\left(\frac{t-u}{s}\right)dt, \tag{1}$$

where s and u being the scale and translation parameters of the mother wavelet $\psi(t)$, which defines the wavelet family function as $\psi_{u,s}(t)=\frac{1}{\sqrt{s}}\psi(\frac{t-u}{s})$. In our study, in order to characterize both amplitude and phase of time-domain magnetoresistive signal [$r(t)$] we use the complex Morlet wavelet family $\psi_{u,s}=\frac{1}{\sqrt{s\pi f_B}}e^{j2\pi f_c(t-u/s)}e^{-(t-u/s)^2/f_B}$ with Fourier spectrum $\Psi_{u,s}(f)=\sqrt{s}e^{-\pi^2 f_B(sf-f_c)^2}e^{-j2\pi uf}$, where f_C and f_B are two parameters [$\Psi(f)$ is the Fourier transform of $\psi(t)$]. The use of a wavelet analysis allows to characterize a signal in the time-frequency space to study the nonstationary behavior (for a complete review of wavelet theory see Refs. 24 and 25). The f_B (called bandwidth parameter) can rule the band of the complex Morlet Fourier spectrum giving narrowed band as it increases. Consequently this parameter is correlated with the frequencies we have to analyze independently of each other. Furthermore for practical reasons f_B and f_C have to be large enough to make the mean of $\psi(t)$ arbitrarily small.[26]

Our results suggest that the continue wavelet transform $W_r(u,s)$ shows better statistical performance than any other time-frequency analysis methods used to analyze the simulated signals. Figure 2(a) (monotonic line) shows the normalized integrated power spectrum of the voltage signal [inset of Fig. 2(a)]. The slope of this curve increases rapidly close to the high power frequencies f_{P1} and f_{P2} while it increases

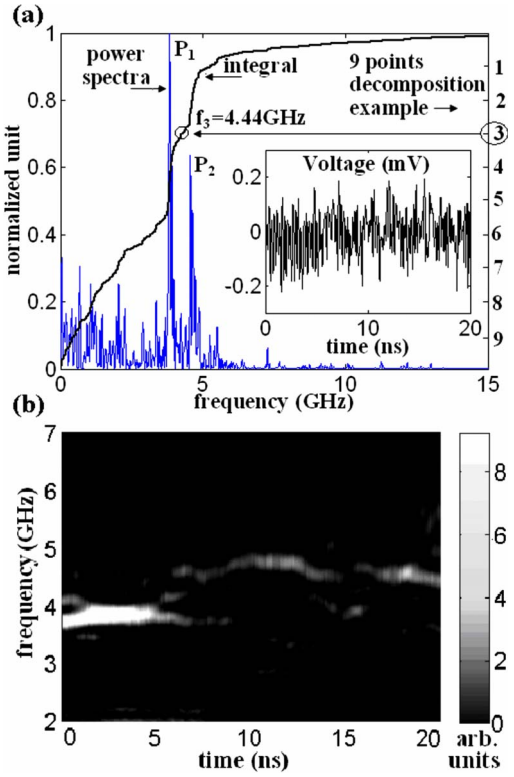

FIG. 2. (Color online) (a) Normalized power spectrum and integrated power spectrum of voltage signal (inset) measured for $I=4.5$ mA and $H=60$ mT in Ref. 16. The numbers in the right represent an example of nine points decomposition of the y axis to identify the scale set $\{s_i\}_{i=1\ldots9}$ for the wavelet transform. (b) Wavelet scalogram of the voltage signal displayed in the inset of Fig. 2(a).

slowly elsewhere (depending on the noise in the power spectrum). Given a fixed dimension N of a scale set $\{s_i\}_{i=1\ldots N}$ for the wavelet family, the y axis is divided in $N+2$ points [Fig. 2(a) shows a decomposition for $N=9$, see the number in the right] and from each point a frequency f_i and a scale s_i can be obtained (e.g., for the number 3, $f_3=4.44$ GHz and $s_3=f_S/f_3$, $f_S=30$ GHz being the sampling frequency).

The best way to show the time-frequency characterization of a signal is the wavelet scalogram (WS). Furthermore the integral of the WS of a signal over the time can be correlated with the Fourier spectrum of that signal directly for a fixed scale parameter.[27] The WS of $r(t)$ is defined as $P_W^r(t,f)=|W_r(u,s)|^2$, the time t being the center value of the wavelet translated by u and the frequency f is computed directly by the scale factor as $f=f_S/s$, f_S being the sampling frequency (rigorously speaking f is the scale frequency and in general it is different from the Fourier frequency, but for the complex Morlet wavelet with $f_C=1$ the two frequencies are nearly identical).[28]

Figure 2(b) shows the WS (arbitrary units) computed for the voltage signal of the inset of Fig. 2(a). We use the following parameters: $N=22$, $f_B=300$, and $f_C=1$. As can be noted, the results of our computations are consistent with the data displayed in Fig. 6 of Ref. 16.

To perform time-frequency analysis of micromagnetic simulations, we introduce a generalization of the micromagnetic spectral mapping technique (MSMT) (Refs. 29 and 30) the micromagnetic WS (MWS). The MWS is the sum over all the computational cells (N_C) of the WS of the magnetoresistance temporal evolution computed for each cell $W_r^i(u,s)$,

$$P_W^r(t,f)=\frac{1}{N_C}\sum_{i=1}^{N_C}P_W^{r_i}(t,f) \tag{2}$$

The scale set $\{s_i\}_{i=1\ldots Nc}$ is determined directly by the spectrum computed with the MSMT with the procedure described above [see Fig. 2(a)]. In general, this study can be also performed for each component of the magnetization. Figure 3 shows (a) the MWS ($N=22, f_B=10^3$), (b) the power spectrum computed by the MSMT, and (c) the temporal evolution of the normalized magnetoresistance signal $r(t)$ for the following value of current density (J), external field (H), and temperature (T): $J=1.5\times10^8$ A/cm^2, $H=60$ mT applied along $-45°$ with respect to the easy axis, and $T=300$ K.

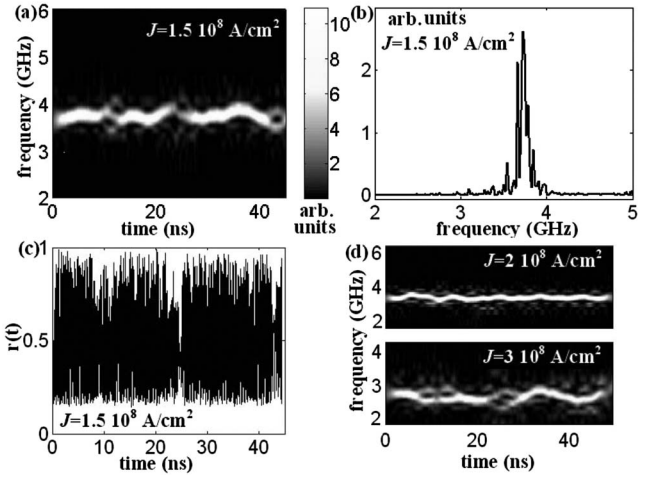

FIG. 3. Theoretical computations for $J=1.5\times10^8$ A/cm^2, $H=60$ mT applied along $-45°$ with respect to the easy axis, and $T=300$ K of (a) micromagnetic wavelet scalogram ($N=22$), (b) the power spectrum computed by the micromagnetic spectral mapping technique, and (c) the temporal evolution of the normalized magnetoresistance signal $r(t)$ computed by numerically solving the Landau-Lifshitz-Gilbert-Slonczewski as described in the text. (d) micromagnetic wavelet scalogram computed for same field and temperature of (a) and for (top) $J=2\times10^8$ A/cm^2 and (bottom) $J=3\times10^8$ A/cm^2. The color bar of (d) is the same of (a).

The MWS is able to detect the intermittent features of the $r(t)$ [for example, Fig. 3(a) $t\approx9$ ns and $t\approx25$ ns), a characteristic which cannot be find out via Fourier analysis. Our numerical experiment shows several interesting results. The excited modes of a spin-torque nano-oscillator are turned off (for nanosecond interval) in an intermediate static magnetic configuration characterized by output very small power (intermittent nonperiodic behavior) and then re-excited. The magnetization dynamics is characterized by a main mode with a frequency which moves in time in a range of a few hundreds of megahertz at least. This mechanism sets the minimum value of the linewidth of the mode. This frequency modulation has been also predicted by stochastic nonlinear theory.[21] As the current increases, first a region in which the

intermittences disappear [see Fig. 3(d) top which shows the MWS for $J=2\times10^8$ A/cm^2] then a region where the intermittences reappear [see Fig. 3(d) bottom which shows the MWS for $J=3\times10^8$ A/cm^2]. This gives rise at least to a linewidth broadening with a Lorentzian shape added to the ideal power spectrum.[31,32]

This wavelet-based analysis together with micromagnetic simulations is able to investigate completely the time-frequency behavior of magnetization dynamics from LLGS equation including the transient dynamics in magnetization switching processes and the existence of persistent but non-periodic current-driven magnetic states. From a more general point of view, it can be used to analyze all the physical problems where a systematic nonstationary analysis has to be performed.

IV. CONCLUSION

In conclusion, experiments and simulations of nanoscale exchange-biased spin-valves show very rich dynamical behavior. At high nonlinear dynamical regime, even though the frequency of the main excited mode decreases monotonically as function of current, the integrated output power shows non-monotonic behavior with a minimum related to a change in the oscillation axis of the magnetization. This is a crucial point to take into account in the design of spin-torque nano-oscillators.

By combining micromagnetic simulations and time-frequency characterization of the magnetization dynamics, we observe together a frequency modulation, current-dependent nanosecond intermittent disappearing and reappearing of the magnetization dynamics, and the instantaneous microwave output power. This aspect has to taken into account to improve theoretical prediction of linewidth of a spin-torque nano-oscillator.

This work was partially supported by Spanish Project under Contracts No. MAT2008-04706/NAN and No. SA025A08.

*Corresponding author; gfinocchio@ingegneria.unime.it

[1] J. Slonczewski, J. Magn. Magn. Mater. **159**, L1 (1996).
[2] L. Berger, Phys. Rev. B **54**, 9353 (1996).
[3] M. Tsoi, A. G. Jansen, J. Bass, W. C. Chiang, V. V. Tsoi, and P. Wyder, Nature (London) **406**, 46 (2000).
[4] J. A. Katine, F. J. Albert, R. A. Buhrman, E. B. Myers, and D. C. Ralph, Phys. Rev. Lett. **84**, 3149 (2000).
[5] J. Grollier, V. Cros, A. Hamzic, J. M. George, H. Jaffrès, A. Fert, G. Faini, J. Ben Youssef, and H. Legall, Appl. Phys. Lett. **78**, 3663 (2001).
[6] S. Urazhdin, N. O. Birge, W. P. Pratt, and J. Bass, Phys. Rev. Lett. **91**, 146803 (2003).
[7] S. I. Kiselev, J. C. Sankey, I. N. Krivorotov, N. C. Emley, R. J. Schoelkopf, R. A. Buhrman, and D. C. Ralph, Nature (London) **425**, 380 (2003).
[8] I. N. Krivorotov, N. C. Emley, J. C. Sankey, S. I. Kiselev, D. C. Ralph, and R. A. Buhrman, Science **307**, 228 (2005).
[9] W. H. Rippard, M. R. Pufall, S. Kaka, S. E. Russek, and T. J. Silva, Phys. Rev. Lett. **92**, 027201 (2004).
[10] A. A. Tulapurkar, Y. Suzuki, A. Fukushima, H. Kubota, H. Maehara, K. Tsunekawa, D. D. Djayaprawira, N. Watanabe, and S. Yuasa, Nature (London) **438**, 339 (2005).
[11] J. A. Katine and E. E. Fullerton, J. Magn. Magn. Mater. **320**, 1217 (2008).
[12] J. Z. Sun and D. C. Ralph, J. Magn. Magn. Mater. **320**, 1227 (2008).
[13] T. J. Silva and W. H. Rippard, J. Magn. Magn. Mater. **320**, 1260 (2008).
[14] K. V. Thadani, G. Finocchio, Z.-P. Li, O. Ozatay, J. C. Sankey, I. N. Krivorotov, Y.-T. Cui, R. A. Buhrman, and D. C. Ralph, Phys. Rev. B **78**, 024409 (2008).
[15] I. N. Krivorotov, D. V. Berkov, N. L. Gorn, N. C. Emley, J. C. Sankey, D. C. Ralph, and R. A. Buhrman, Phys. Rev. B **76**, 024418 (2007).
[16] I. N. Krivorotov, N. C. Emley, R. A. Buhrman, and D. C. Ralph, Phys. Rev. B **77**, 054440 (2008).
[17] P. P. Horley, V. R. Vieira, P. M. Gorley, V. K. Dugaev, and J. Barnas, Phys. Rev. B **77**, 094427 (2008).
[18] L. Torres, L. Lopez-Diaz, E. Martinez, M. Carpentieri, and G. Finocchio, J. Magn. Magn. Mater. **286**, 381 (2005).
[19] G. Finocchio, I. N. Krivorotov, M. Carpentieri, G. Consolo, B. Azzerboni, L. Torres, E. Martinez, and L. Lopez-Diaz, J. Appl. Phys. **99**, 08G507 (2006); G. Finocchio, M. Carpentieri, B. Azzerboni, L. Torres, E. Martinez, and L. Lopez-Diaz, *ibid.* **99**, 08G522 (2006).
[20] J. C. Goswami and A. K. Chan, *Fundamentals of Wavelets. Theory, Algorithms and Applications* (Wiley, New York, 2000).
[21] J.-V. Kim, Phys. Rev. B **73**, 174412 (2006).
[22] G. Siracusano, G. Finocchio, I. N. Krivorotov, L. Torres, G. Consolo, and B. Azzerboni, J. Appl. Phys. **105**, 07D107 (2009); G. Finocchio, I. N. Krivorotov, L. Torres, R. A. Buhrman, D. C. Ralph, and B. Azzerboni, Phys. Rev. B **76**, 174408 (2007).
[23] J. Slonczewski, J. Magn. Magn. Mater. **247**, 324 (2002).
[24] I. Daubechies, *Ten Lectures on Wavelets*, CBMS-NSF Regional Conference Series in Applied Mathematics (SIAM, Philadelphia, 1992).
[25] S. Mallat, *A Wavelet Tour of Signal Processing* (Academic, San Diego, 1998).
[26] N. Delprat, B. Escudie, P. Guillemain, R. Kroland-Martinet, P. Tchamitchian, and B. Torresani, IEEE Trans. Inf. Theory **38**, 644 (1992).
[27] L. Hudgins, C. A. Friehe, and M. E. Mayer, Phys. Rev. Lett. **71**, 3279 (1993).
[28] C. Torrence and G. P. Compo, Bull. Am. Metereol. Soc. **79**, 61 (1998).
[29] R. D. McMichael and M. D. Stiles, J. Appl. Phys. **97**, 10J901 (2005).
[30] L. Torres, L. Lopez-Diaz, E. Martinez, G. Finocchio, M. Carpentieri, and B. Azzerboni, J. Appl. Phys. **101**, 053914 (2007).
[31] S. Machlup, J. Appl. Phys. **25**, 341 (1954).
[32] M. R. Pufall, W. H. Rippard, Shehzaad Kaka, S. E. Russek, T. J. Silva, J. Katine, and M. Carey, Phys. Rev. B **69**, 214409 (2004).